



**HAL**  
open science

# Spectral shapes of rovibrational lines of CO broadened by He, Ar, Kr and SF 6: A test case of the Hartmann-Tran profile

H. Ngo, H. Lin, J.T. Hodges, H. Tran

► **To cite this version:**

H. Ngo, H. Lin, J.T. Hodges, H. Tran. Spectral shapes of rovibrational lines of CO broadened by He, Ar, Kr and SF 6: A test case of the Hartmann-Tran profile. *Journal of Quantitative Spectroscopy and Radiative Transfer*, 2017, 10.1016/j.jqsrt.2017.03.001 . hal-01484556

**HAL Id: hal-01484556**

**<https://hal.sorbonne-universite.fr/hal-01484556>**

Submitted on 7 Mar 2017

**HAL** is a multi-disciplinary open access archive for the deposit and dissemination of scientific research documents, whether they are published or not. The documents may come from teaching and research institutions in France or abroad, or from public or private research centers.

L'archive ouverte pluridisciplinaire **HAL**, est destinée au dépôt et à la diffusion de documents scientifiques de niveau recherche, publiés ou non, émanant des établissements d'enseignement et de recherche français ou étrangers, des laboratoires publics ou privés.

## Spectral shapes of rovibrational lines of CO broadened by He, Ar, Kr and SF<sub>6</sub>: A test case of the Hartmann-Tran profile

N. H. Ngo<sup>1</sup>, H. Lin<sup>2,3</sup>, J.T. Hodges<sup>2</sup>, H. Tran<sup>4\*</sup>

\*Corresponding author: htran@lmd.jussieu.fr

<sup>1</sup> Faculty of Physics, Hanoi National University of Education, 136 Xuan Thuy, Cau Giay, Hanoi, Vietnam

<sup>2</sup> National Institute of Standards and Technology, 100 Bureau Drive, Gaithersburg, MD 20899, USA

<sup>3</sup> National Institute of Metrology, Beijing 100029, China

<sup>4</sup> Laboratoire de Météorologie Dynamique, IPSL, CNRS UMR 8539, Sorbonne Universités, UPMC Univ. Paris 06, 75252 Paris, France

### Abstract

High signal-to-noise ratio spectra of the (3-0) band P(1) and P(17) lines of CO broadened by He, Ar, Kr and SF<sub>6</sub> were measured with a frequency-stabilized cavity ring-down spectroscopy system. For each collision-partner and both lines, multiple spectra were measured over pressures spanning nearly three decades up to 130 kPa. These data were analyzed with a multispectrum fitting procedure. Line shapes were modeled using the Hartmann-Tran (HT) profile with first-order line mixing as well as several other simplified profiles. The results show that for all considered collision partners (with the exception of SF<sub>6</sub>), the HT profile captures the measured line shapes with maximum absolute residuals that are within 0.1% of the peak absorption. In the case of SF<sub>6</sub>, which is the heaviest perturber investigated here, the maximum residuals for the HT profile are twice as large as for the other collision partners.

Keywords:

CO, line shape, Hartmann-Tran profile, cavity ring-down spectroscopy

## 1. Introduction

Carbon monoxide (CO) is one of the most abundant trace gases in the atmosphere of the Earth. It is also present in planetary and stellar atmospheres as well as in the interstellar medium. As indicated by the large number of papers devoted to its spectroscopy (see [1] and references therein), CO is one of the most frequently measured diatomic molecules using spectroscopic techniques. In addition to line position and intensity measurements, line shapes of CO transitions in the rotational, fundamental as well as overtone bands also have been the subject of several studies. Also, because CO is a simple diatomic molecule, it is a useful system for evaluating theoretical profiles and for testing intermolecular potential parameters. Many papers [2–14] have been devoted to studies of N<sub>2</sub>, O<sub>2</sub> and air broadening of CO lines for atmospheric remote sensing applications. The He-broadening of CO transitions was also extensively studied [4,5,8,13,15–25] because this case is relevant to determining the composition of interstellar molecular clouds and the atmospheres of the outer planets. Also, many other rare gases have been considered as collision partners to investigate how CO line shapes depend on the perturber-to-absorber mass ratio [4,5,7,13,16,19,20,23,26–36]. All of these studies indicate that measured CO line shapes deviate from the often-used Voigt profile. Given that deviations between theory and experiment can reach a few percent of the peak absorption, increasingly demanding applications such as remote sensing of the Earth's atmosphere require improved models that account for higher-order effects influencing the line shape. These effects include: collisional-induced velocity changes (Dicke narrowing effect [37]), speed dependence of the collisional width and shift, correlation between velocity- and internal-state-changing collisions and collisional interference between lines (line mixing). Depending on the specific molecular system, line and pressure range under consideration, all or some of these effects may be important. For isolated lines (no line mixing), various non-Voigt models have been used to represent the measured spectra. These include the Galatry (soft-collision model) [38] and Rautian (or Nelkin-Ghatak, hard-collision model [39,40]) profiles for the Dicke narrowing, the speed dependent Voigt profile [41] for the speed dependence effect, and finally the speed dependent hard- or soft-collision model which accounts for speed dependence and Dicke narrowing. The choice of line profile used in the data reduction can have a large influence on retrieved parameters. For example, the fitted line broadening parameter can be sensitive to the choice of line profile used in the model.

For CO, a number of line profiles have been used to model the measured spectra, although only some studies devoted to the line shape issue of this molecule are recalled here. In Ref. [3], Duggan et al. used a combination of the soft-collision model for the translational degrees of freedom and a simple exponential decay for the optical coherence to fit measured spectra of CO lines in N<sub>2</sub>. They showed that the fitted narrowing parameter (also called the optical frequency of velocity-changing collisions) is not linear with pressure and the corresponding optical diffusion constant could be up to several times smaller than that deduced from mass diffusion. When fixing the narrowing coefficient to that calculated from the mass diffusion constant, they observed that the time correlation function for the evolution of the optical coherence could not be described by a simple exponential decay. In Ref. [4], this deviation was attributed to the speed dependence of the line broadening. Consequently, a combination of soft-collision and speed dependence models [42] was fit to measured spectra of CO broadened by He, N<sub>2</sub> and Xe. In a similar fashion, a model given by the convolution of hard-collision and speed dependence [42] profiles was also fit to measured spectra of CO with various collision-partners [5,7]. The speed dependent Galatry profile proposed in [43] was used to model measured spectra of CO in He and Ar [19]. The authors claimed that this model is not sufficient for CO in Ar. Rather, one may need to account for the correlation between velocity-changing and dephasing collisions. Finally, in Refs. [31,32] the speed dependent billiard-ball model was compared to measured spectra of CO in Ar. This analysis requires accurate calculations for the speed dependent width and shift and assumes a hard-sphere model for velocity-changing collisions. Although leading to very good agreement with measured spectra [32], this model is too computationally intensive and unsuitable for applications such as radiative transfer calculations.

The IUPAC recently recommended the use of the Hartmann-Tran profile (HTp) for high resolution spectroscopy [44,45] as a reference line profile for data analysis. This profile is a version of the correlated speed-dependent Rautian profile of Pine [46] with the speed-dependence of collisional width and shift given in the quadratic form proposed by Rohart et al. [9,47]. The HTp profile takes into account Dicke narrowing, speed dependence effects and correlation between velocity-changing and internal-state-changing collisions. In addition, collisional interferences between lines can be easily introduced by invoking the first-order approximation of Rosenkranz [44,48,49]. Importantly, this profile can be computed nearly as rapidly as the Voigt profile. Several tests with some molecular systems showed that this profile can describe the measured

line shape with a precision of about  $\pm 0.1\%$  of the peak absorption (see [45] and references therein). Because of the large number of parameters (i.e. at a given temperature, one needs four parameters for the line width, shift and their speed dependences, one parameter to represent the Dicke narrowing, and one parameter for the velocity and internal-state changing collision correlation), and because of numerical correlations between some of these parameters, high signal-to-noise spectra recorded over a wide pressure range are required for precise parameter retrieval [44,45]. To the best of our knowledge, no validation of the HT profile under such conditions has been performed for CO with various collision partners.

In this work, we quantify how well the HT profile models foreign-broadened CO line shapes. Room temperature data were acquired for broadening by gases of different mass (He, Ar, Kr, SF<sub>6</sub>) taken over a pressure range spanning three decades. High signal-to-noise spectra of the P(1) and P(17) lines in the (3-0) vibrational band of <sup>12</sup>C<sup>16</sup>O mixed with each of these collision-partners were measured with a frequency-stabilized cavity ring-down spectroscopy (FS-CRDS) apparatus, developed at the National Institute of Standard and Technology (NIST) in Gaithersburg. These spectra were analyzed using multispectrum fitting of the line shape model to the measured spectra, whereby the model parameters were adjusted simultaneously for all pressure conditions.

In the remainder of this article, we describe the FS-CRDS measurements and the analysis procedure (Sec.2). The fitting results and the obtained line parameters are reported and discussed in Sections 3 and 4 while conclusions and related perspectives are given in Sec. 5.

## 2. Experimental details and spectrum analysis

A detailed description of the present system, which is based on the original FS-CRDS spectrometer discussed in Ref. [50], can be found in Ref. [51]. Only an overview of the experiment will be given here. The central feature of the cavity ring-down spectrometer is an actively length-stabilized optical resonator within a vacuum chamber. The resonator comprises two high-finesse, double-coated ( $F = \pi/(1-R) = 108,000$  near  $\lambda = 1570$  nm where  $R$  is the intensity reflectivity, and  $F=60$  near  $\lambda = 633$  nm) spherical mirrors separated by  $L=139$  cm. The optical resonator length is stabilized in a closed-loop-servo configuration by maximizing the transmission of an I<sub>2</sub>-stabilized HeNe reference laser which has a long term stability of  $\pm 10$  kHz. Actuation of the cavity length is achieved by displacing one of the resonator mirrors with a piezoelectric device. The probe laser beam is emitted by a single-frequency ( $< 500$  kHz short-term bandwidth) continuous-wave external cavity diode laser which is amplified to

30 mW of power by a booster-optical amplifier (BOA) and mode-matched into the ring-down cavity. At each frequency step, the probe laser frequency was actively locked to a cavity TEM<sub>00</sub> mode, with the starting frequency of each scan measured to within 100 kHz by comparison to a Cs-clock-referenced optical frequency comb (OFC) as described in Ref. [51].

Ring-down events were initiated by using the BOA as an optical switch to extinguish the probe laser beam. 320 decay signals per frequency step were measured with an InGaAs detector/photoreceiver and digitized with a 16-bit board at a sampling rate of 10 Msamples s<sup>-1</sup>. In order to determine the cavity decay time  $\tau$ , the signals were modeled using the three-parameter function  $s(t) = Ae^{-t/\tau} + y_b$  where  $A$  is the signal amplitude at time  $t=0$  and  $y_b$  is the baseline offset. This exponential model was fit to each ring-down decay signal by varying all three parameters, yielding a distribution of measured time constants at each frequency step characterized in terms of a mean value  $\bar{\tau}$  and standard deviation  $\sigma_\tau$ . We obtained acquisition rates of 150 Hz at each frequency step, and fractional uncertainties  $\sigma_\tau / \bar{\tau} = 0.04\%$  resulting in an empty-cavity noise-equivalent absorption coefficient (NEA) of  $7 \times 10^{-12} \text{ cm}^{-1} \text{ Hz}^{-1/2}$  and minimum detectable absorption of  $5 \times 10^{-12} \text{ cm}^{-1}$ .

Absorption spectra were acquired by step-wise tuning the laser frequency through successive longitudinal modes  $q$  of the ring-down cavity which are separated by the cavity free spectral range  $\nu_f$ , nominally equal to 109 MHz. In order to account for variations in  $\nu_f$  with gas density and composition, the mode spacing was measured for each spectrum using the OFC at the beginning and end of the scan and by counting mode orders. This method yielded an uncertainty of less than 5 kHz in  $\nu_f$  for all spectra.

The total loss-per-unit length of a ring-down cavity equals the sum of the base losses associated with the high-reflectivity mirrors  $\alpha_0 = (1-R)/L$ , the frequency-dependent absorption coefficient of the sample  $\alpha_{ab}(\Delta\nu_q)$ , and other weak and slowly varying losses such as Rayleigh scattering that can be combined with the mean mirror losses  $\bar{\alpha}_0$ . Here  $\Delta\nu_q = \Delta q\nu_f$  is the frequency detuning relative to the first point of the spectrum. The base losses also exhibit sinusoidal oscillations (etalons) about  $\bar{\alpha}_0$  given by  $\alpha_{et}(\Delta\nu_q)$  which are caused by coupled-cavity effects [52]. In the present study, the dominant etalon had a period of 26 GHz with an amplitude  $10^{-9} \text{ cm}^{-1}$ , which is approximately 0.5% of  $\bar{\alpha}_0$ . This

subtle feature in the spectrum baseline is caused by etaloning between the planar and concave surfaces of the 4-mm-thick ring-down cavity mirrors. With the foregoing definitions, measured spectra were modeled by

$$\frac{1}{c\bar{\tau}(\Delta\nu_q)} = \bar{\alpha}_0 + \alpha_{et}(\Delta\nu_q) + \alpha_{ab}(\Delta\nu_q) \quad (1)$$

in which  $c$  is the speed of light. Measurements of the cavity free spectral range, mode-order difference  $\Delta q$ , and decay rates  $\tau^{-1}$ , thus provided the  $x$  and  $y$  axes of the spectra, respectively. Using this approach, the spectrum axes were directly obtained in terms of precise and accurate observations of laser frequency and ring-down decay time.

Absorption spectra were acquired at room temperature on samples comprising binary mixtures of high-purity (99.998 %) CO diluted by the He, Ar, Kr and SF<sub>6</sub> buffer gases. To this end, a small amount of CO (300 Pa – 450 Pa) was introduced into the evacuated cavity and back-filled with each buffer gas to a maximum pressure close to atmospheric pressure. This technique resulted in CO molar fractions spanning 0.25 % to 0.4 %. For each binary mixture, spectra of the P(1) and P(17) lines were acquired for 6 to 9 static pressure conditions, beginning at the maximum pressure and stepwise pumping to lower pressures. The resulting measurement conditions ranged from 0.13 kPa to 130 kPa and are given in Table 1.

Table 1: Experimental conditions for the measured spectra of the P(1) and P(17) lines in the (3-0) band of <sup>12</sup>C<sup>16</sup>O diluted by He, Ar, Kr and SF<sub>6</sub>. The corresponding  $\Gamma_L/\Gamma_D$  values are also reported (with  $\Gamma_L$ ,  $\Gamma_D$  respectively the estimated Lorentz and the calculated Doppler widths). The pressures and molar fractions are nominal values, with the latter estimated from the peak areas and line intensities.

Perturber	Line	Pressure (kPa)	$\Gamma_L/\Gamma_D$	CO molar fraction
He	P(1)	1.3, 3.3, 6.7, 10, 13, 33, 67, 100, 127	0.088-8.39	$2.5 \times 10^{-3}$
	P(17)	1.3, 3.3, 6.7, 10, 13, 33, 67, 100, 127	0.085-8.03	

Ar	P(1)	1.3, 6.7, 13, 33, 67, 100, 127	0.128-12.19	$3.0 \times 10^{-3}$
	P(17)	1.3, 6.7, 13, 33, 67, 100, 127	0.078-7.45	
Kr	P(1)	1.3, 6.7, 13, 33, 67, 100	0.138-10.38	$3.3 \times 10^{-3}$
	P(17)	1.3, 6.7, 13, 33, 67, 100	0.079-5.89	
SF <sub>6</sub>	P(1)	0.13, 1.3, 6.7, 13, 33, 67, 100, 127	0.018-17.64	$3.6 \times 10^{-3}$
	P(17)	0.13, 1.3, 3.3, 6.7, 13, 33, 67, 100, 127	0.012-11.68	

The measured spectra were fit using the HT profile and with simplified models: the speed dependent hard collision model (SDHC [53]), the speed dependent Voigt profile (SDV), the hard- and soft-collision models (HC and SC) and the Voigt profile (V). The quadratic forms [9,45,47] for the speed dependences of the line width and shift were used, i.e.:  $\Gamma(\nu) + i\Delta(\nu) = \Gamma_0 + i\Delta_0 + (\Gamma_2 + i\Delta_2)[(\nu/\tilde{\nu})^2 - 3/2]$  where  $\tilde{\nu} = \sqrt{2k_B T/m}$  is the most probable speed for an absorbing molecule of mass  $m$ . Detailed expressions of these profiles can be found in [44] and references therein. For the HT profile, the normalized  $I^{HT}(\sigma)$  line shape is a function of eight parameters [44],

$$I_{HTP}(\sigma) = f(\sigma - \sigma_0, \Gamma_D, \Gamma_0, \Gamma_2, \Delta_0, \Delta_2, \nu_{vc}, \eta), \quad (2)$$

where  $\sigma_0$  is the unperturbed position of the line,  $\Gamma_D$  is the Doppler broadening,  $\nu_{vc}$  is the frequency of velocity-changing collisions (the Dicke narrowing effect, described by the hard-collision limit within the HT profile) and  $\eta$  is the correlation parameter which accounts for temporal correlation between velocity-changing and internal-state-changing collisions. The line parameters of the HT profile vary simply with the total pressure  $P$ :  $\sigma_0$ , and  $\eta$  are constant while  $\nu_{vc}$ ,  $\Gamma_0$ ,  $\Gamma_2$ ,  $\Delta_0$  and  $\Delta_2$  are proportional to  $P$ . Note that the SDHC model is obtained from Eq. (2) when  $\eta$  is set to zero. When  $\eta = \nu_{vc} = 0$ , we obtain the SDV profile while Eq. (2) becomes the HC model when  $\eta = \Gamma_2 = \Delta_2 = 0$ . Finally, the Voigt profile is obtained if all higher-order line shape parameters are zero ( $\eta = \nu_{vc} = \Gamma_2 = \Delta_2 = 0$ ). In addition, the line mixing (LM) effect has also

been taken into account in our fits through the use of the first-order approximation [44,49]. With this assumption, the magnitude of the first-order line mixing effect is given by the (pressure dependent) coefficient  $Y$ .

For each line and for a given perturber, a set of calculated line profiles was simultaneously fit to multiple spectra (measured at various pressures) by global least-squares adjustment of the fitted parameters, similarly to the multispectrum fitting technique of Ref. [54]. The set of shared parameters (i.e. those considered for all pressures) were:  $\sigma_0, \gamma_0, \gamma_2, \delta_0, \delta_2, \beta, \eta, \frac{Y}{P}$  with  $\gamma_0 = \frac{\Gamma_0}{P}, \gamma_2 = \frac{\Gamma_2}{P}, \delta_0 = \frac{\Delta_0}{P}, \delta_2 = \frac{\Delta_2}{P}$  and  $\beta = \frac{v_{vc}}{P}$ . For each spectrum, the integrated line intensity and a linear baseline (with etalon) representing the zero absorption level was also retrieved. All fitted spectra shown below were normalized to have a peak absorption of unity (dimensionless) at line center. The Doppler contribution was calculated from the measured temperature and frequency for each transition and then held constant during the fits.

### 3. Fit residuals and obtained parameters

#### 3.1 CO-He

Figure 1 presents the fit residuals obtained by fitting the two considered lines of CO broadened by He with various line shape models. Note that for the non-Voigt profiles, only the results obtained with line mixing are presented. Spectral fits with these profiles and without line mixing were carried out but are not plotted here. The obtained parameters for each model are reported in Table 2. We can observe that the value of the line-mixing parameter ( $Y/P$ ) is nearly independent of the line shape model used. Comparison of these values and the fit residuals obtained with and without (not shown here) line mixing show that line mixing for the P(1) line is more important than for the P(17) line. As expected, the Voigt profile leads to the worst fit residuals in comparison to the results obtained with the other profiles. Considering only the Dicke narrowing effect, the SC model leads to much better results than does the HC model. This is consistent with theoretical predictions [38,55] which show that the SC model is more suitable than the HC model when the active molecule is much heavier than the perturber. The remaining residuals can be explained by the contribution of the speed dependence effect, which is neglected by the SC and HC models. The speed dependent Voigt profile leads to good fits of the measured spectra, with fit residuals being almost within the experimental noise below 0.1% of the peak absorption. Note

that comparison between the various profiles can be also done through the standard deviation of the fits (i.e. rms) as reported in Table 2. As discussed in [19] for the CO/He system, the characteristic decay time of the optical coherence, given by  $1/2\pi\Gamma_0$  (with  $\Gamma_0 \approx 1.4$  GHz at 100 kPa), is seven-fold smaller than the relaxation time of the velocity, given by  $1/2\pi\nu_{VC}$  ( $\nu_{VC} = 0.2$  GHz at 100 kPa). This quantity is the rate of velocity-changing collisions based on the mass diffusion coefficient which is calculated using a simple Lennard-Jones potential with parameters given in [56]. In this case, we can safely assume that the correlation between velocity-changing and internal-state-changing collisions is negligible. With this assumption, the HT profile reduces to the SDHC model (by fixing  $\eta = 0$  in Eq. (2)). The latter is then used to fit the measured spectra of CO in He. As can be observed in Fig. 1, the fit residuals in this case are slightly improved with respect to the SDV profile and completely within the experimental noise. The fitted Dicke narrowing parameter (see Table 2) is close to zero showing that the contribution of this effect should be small for CO in He. Consequently, the measured spectra of CO in He over the considered pressure range can be precisely modeled using the SDV profile.

### 3.2 CO-Ar

The results obtained for CO in Ar are plotted in Figure 2. The observed non-Voigt effects for this system are much more important than for CO in He, as was also discussed in Refs. [13,19]. For the two lines considered here, the HC and SC models give similar fit residuals. The SDV profile leads to better fit residuals than the HC and SC models for the P(1) line whereas for the P(17) line, the opposite situation is observed. Obviously, both speed dependence and velocity-changing collision effects contribute to the line shape because none of the SDV, HC and SC models result in a perfect fit to the measured spectra. The mass-diffusion-coefficient-derived value  $\beta_0 = 7.25$  kHz/Pa, which characterizes the velocity relaxation, is more comparable to the value of  $\gamma$  (see Table 2) than for the case of CO in He. Consequently and consistent with the claim in Ref. [19], we expect that the correlation between velocity-changing and internal-state-changing collisions should contribute to the line shape of CO in Ar. When fitting measured spectra of CO in Ar with the HT profile, we fit all the line shape parameters, including the Dicke narrowing. Note that, in some studies, because of the limited signal-to-noise ratio and/or a narrow pressure range, the Dicke narrowing parameter  $\beta = \frac{\nu_{VC}}{P}$  is often fixed to  $\beta_0$  in order to decrease the number of floated parameters (e.g. [57,58]). This approximation can be safely used for systems for

which the relative contribution of the Dicke narrowing effect to the line shape is small. However, in the general case, because of the different approximations made in derivation of the HT profile (quadratic speed dependences of the line width and shift, hard collisions for the velocity changes), the value of  $\beta$  beta should not be equal to  $\beta_0$ .

For the P(1) line, the value of  $\beta$  retrieved with the HT profile (see Table 2) is close to  $\beta_0$ . The much better fit residuals obtained with the HT profile (better than  $\pm 0.1\%$ ) with respect to those obtained with the SDHC demonstrates that the correlation between velocity- and internal-state-changing collisions has to be taken into account. These results are consistent with the very recent work of [59] which also shows that the HTp leads to better fit of spectra of CO in Ar than the SDHC. For the P(17) line, the HT and SDHC profiles lead to similar fit residuals and line shape parameters.

### 3.3 CO-Kr and CO-SF<sub>6</sub>

The results obtained for CO in Kr and in SF<sub>6</sub> are plotted in Figures 3 and 4, respectively. These results are quite similar to those of CO in Ar. For these two collision-partners (as for the CO-Ar case) the SDV profile gives better fit residuals than do the hard- and soft-collision models for the P(1) line. However, for the P(17) line the HC and SC models lead to slightly better fits to the data than does the SDV profile (see also the values of the root mean square in Table 2). It is clear that with such a large pressure (or  $\Gamma_L/\Gamma_D$ ) range, one needs to account for both the speed dependence and Dicke narrowing to accurately model the observed line shape. The Dicke narrowing parameters deduced from the mass diffusion coefficient are 9.23 and 22.16 kHz/Pa for CO in Kr and SF<sub>6</sub> respectively. These values are comparable to the corresponding values of the line broadening coefficients (see Table 2). Therefore, again, when using the HT profile, we have chosen to fit all the line shape parameters and not to fix the Dicke narrowing parameter to  $\beta_0$ . For the two lines that we considered, the HT profile leads to better fit residuals than does the SDHC model. However, the HT fit residuals are clearly larger than the experimental noise and exhibit relatively large systematic structures, particularly for the P(1) line of CO in SF<sub>6</sub> (up to  $\pm 0.2\%$ ). As shown in Refs. [60,61] for heavy perturbers, the speed dependence effect is increasingly important and the quadratic approximation is probably not sufficiently realistic to describe the speed dependence of the line width and shift. Also, for perturber much heavier than absorber, the hard collision approximation is not adequate for realistic description of velocity changing

collision. To determine the influence of these approximations on the spectral shape, comparison between the HTP results with *ab initio* calculations [62–64] would be helpful.

#### 4. Discussion

For all collision-partners except He, we have shown that the HT profile provides the best fits to the measured spectra by comparison to the other considered profiles. The HT profile can model the measured spectra of CO with these collision-partners over a wide pressure range with a relative precision better than  $\pm 0.2\%$  of the peak absorption. This model accounts for the three principal collisional effects that influence the line shape: velocity-changing collisions, the speed dependences of the line width and shift, and correlation between velocity-changing and internal-state-changing collisions. Because of the different physical approximations used to derive the HTP model such as the hard-collision limit for the collision-induced velocity changes, and the quadratic form for the speed dependence, the resulting line shape parameters should be considered as effective quantities that do not exactly reflect the underlying physics. In the following, we will nevertheless discuss the obtained line shape parameters.

In Table 2, it is evident that the fitted line width strongly depends on the model used. The Voigt profile leads to a smaller line width with respect to the more advanced line shape models. For example, the difference between the line width obtained by Voigt and HT profile can be as much as 8 %. Conversely, the pressure shift is nearly independent of the line shape used, because it is primarily determined by the variation of the peak absorption position with pressure. Fitted values of the speed dependence of the line shift are also independent of the line shape model used (i.e. SDV, SDHC and HT) and are relatively small. As expected, for all considered rare gases (with the exception of the SF<sub>6</sub> P(17) line) the  $\nu_2/\nu_0$  ratio obtained from the SDV and HT profiles increases with the perturber mass, as also observed previously in [13,65]. For the Dicke narrowing parameters, as shown in Table 2, the values obtained with the HT profile increase with the perturber mass. Within the hard-sphere

interaction approximation, this can be explained by the increasing value of the corresponding mean hard-sphere diameter with the perturber mass [56].

From the values of  $\gamma_2$  and  $\gamma_0$  obtained by using the (quadratic) speed dependent profiles, the corresponding hypergeometric speed dependence [i.e.  $\Gamma(v_r) = \Gamma(\bar{v}_r)(v_r/\bar{v}_r)^\alpha$ ] parameters can be deduced using Eq. (11) of [66]. The values of  $\alpha$  can then be related to the empirical collisional interaction potential  $V(r) \sim r^{-q}$  with  $\alpha = \frac{q-3}{q-1}$ . The values of  $q$  can thus be determined and considered as an indicator of the implied interaction potential. For CO in He and for the two lines considered here, from the SDV profile results we found that  $\alpha$  is very close to unity, which corresponds to the case of a hard-sphere interaction ( $q \approx \infty$ ). Similar results are obtained with the SDHC model. The broadening mechanism for CO in He is thus probably mainly caused by the repulsive wall of the potential at short range [56]. This result is also confirmed by the fact that the broadening coefficient of CO in He is nearly independent of the rotational quantum number (see Table 2). For CO in Ar, the value of  $q$ , deduced from the ratio  $\gamma_2/\gamma_0$  obtained with the SDV model, is 5.0 and 7.2 for the P(1) and P(17) lines respectively, while with the HT profile, it is 6.0 and 5.3. This demonstrates that for CO in Ar, the broadening mechanism is mostly driven by the long-range dispersive interaction potential, in opposition to the case of CO in He. For CO in Kr, the value of  $q$  deduced from the  $\gamma_2/\gamma_0$  ratio obtained with the SDV profile is 6.5 and 7.1 for the P(1) and P(17) lines while it is 9.0 and 5.6, respectively for CO in SF<sub>6</sub>. With the HT profile, the value of  $q$  is 16.5 and 6.0 for the P(1) and P(17) lines for CO in Kr whereas it tends to infinity ( $\alpha$  is very close to 1) and is 4.8 for CO in SF<sub>6</sub>. Except for the result obtained with the HT profile for the P(1) line of CO in Kr and SF<sub>6</sub>, these results show that, the long-range dispersive force seems to play a dominant role in the broadening mechanism for CO in Kr and SF<sub>6</sub>.

Table 2: Fitted parameters with the various models used.  $\gamma_0, \gamma_2, \delta_0, \delta_2, \beta$  and  $\beta_0$  are in units of kHz/Pa while  $Y/P$  is in units of  $10^{-5}$  kPa<sup>-1</sup> and  $\eta$  is dimensionless. These quantities can be converted to conventional units using the identity,  $1 \text{ cm}^{-1} \text{ atm}^{-1} = 295.872 \text{ kHz Pa}^{-1}$ . We also report the frequency of velocity-changing collisions  $\beta_0$  is based on the mass diffusion coefficient which is calculated assuming simple Lenard-Jones potentials with parameters given in [56] for each collision-partner. The reported uncertainty, in the same unit of the last digit of the corresponding parameter, is three times the standard deviation given by the fit.

Per	Line	Profile	$\gamma_0$	$\gamma_2$	$\delta_0$	$\delta_2$	$\beta$	$\beta_0$	$\eta$	$Y/P$	rms ( $10^{-3}$ )
He	P(1)	V	14.49(1)		-0.34(2)						1.010
		V+LM	14.48(1)		-0.27(2)					-4.36(36)	0.933
		HC+LM	14.55(1)		-0.27(2)		1.67(3)	1.95		-4.28(10)	0.268
		SC+LM	14.57(1)		-0.27(2)		2.16(3)			-4.26(7)	0.187
		SDV+LM	14.66(1)	0.75(1)	-0.27(2)	0.0				-4.28(5)	0.128
	SDHC+LM	14.65(1)	0.80(1)	-0.27(2)	0.0	-0.12(3)			-4.28(5)	0.126	
	P(17)	V	13.80(1)		-0.41(2)						0.963
		V+LM	13.80(1)		-0.43(2)					1.53(37)	0.952
		HC+LM	13.87(1)		-0.43(2)		1.48(3)	1.95		1.54(8)	0.219
		SC+LM	13.89(1)		-0.43(2)		2.04(3)			1.54(5)	0.121
SDV+LM		13.94(1)	0.70(1)	-0.43(2)	0.03(3)				1.41(4)	0.103	
SDHC+LM		13.93(1)	0.62(1)	-0.43(2)	0.03(3)	0.18(3)			1.42(4)	0.097	
V		20.71(2)		-1.34(3)						1.820	
Ar	P(1)	V+LM	20.71(2)		-1.19(3)					-7.20(56)	1.700
		HC+LM	20.85(1)		-1.19(3)		5.59(20)			-7.15(26)	0.601
		SC+LM	20.87(1)		-1.19(3)		7.07(18)	7.25		-7.13(20)	0.593
		SDV+LM	21.35(1)	2.48(2)	-1.23(2)	-0.09(3)				-6.35(18)	0.205
	SDHC+LM	21.29(1)	2.33(2)	-1.23(2)	-0.09(3)	0.56(15)			-6.39(18)	0.173	
	HT+LM	21.28(1)	2.80(1)	-1.23(2)	-0.12(3)	7.63(6)		0.34(1)	-6.41(9)	0.154	
	P(17)	V	12.42(2)		-2.71(1)						2.710
		V+LM	12.42(2)		-2.70(1)					-0.52(108)	2.710
HC+LM		12.60(1)		-2.70(1)		4.79(15)			-0.39(29)	0.567	
SC+LM		12.63(1)		-2.70(1)		6.33(12)	7.25		-0.37(27)	0.510	
SDV+LM		13.06(1)	1.97(2)	-2.70(1)	0.0				-0.28(30)	0.594	
Kr	P(1)	SDHC+LM	12.88(1)	1.51(1)	-2.70(1)	0.0	1.66(9)			-0.38(20)	0.102
		HT+LM	12.88(1)	1.54(1)	-2.70(1)	0.0	2.22(9)		0.05(1)	-0.38(20)	0.102
		V	21.47(4)		-1.36(13)						0.327
		V+LM	21.46(4)		-1.21(11)					-9.99(177)	0.322
		HC+LM	21.87(2)		-1.21(11)		8.58(36)			-9.49(66)	0.122
	P(17)	SC+LM	21.92(2)		-1.21(11)		10.86(44)	9.23		-9.43(69)	0.129
		SDV+LM	23.24(1)	4.19(1)	-1.30(12)	-0.15(3)				-6.58(21)	0.383
		SDHC+LM	23.13(1)	4.02(1)	-1.30(12)	-0.15(3)	0.80(9)			-6.72(17)	0.310
		HT+LM	22.96(1)	5.57(1)	-1.30(12)	-0.18(3)	13.52(6)		0.58(1)	-7.07(8)	0.165
		V	12.24(3)		-3.70(4)				9.23		38.600

	V+LM	12.24(3)		-3.67(4)				-0.69(249)	38.600	
	HC+LM	12.54(1)		-3.67(4)		6.24(15)		-1.40(45)	0.709	
	SC+LM	12.59(1)		-3.66(3)		8.17(15)		-1.51(45)	0.713	
	SDV+LM	13.23(1)	2.51(2)	-3.66(3)	0.03(3)			-2.31(61)	0.962	
	SDHC+LM	12.92(1)	1.85(1)	-3.66(3)	0.03(3)	2.40(3)		-2.10(13)	0.204	
	HT+LM	12.91(1)	2.20(1)	-3.66(3)	0.03(3)	6.39(3)	0.32(1)	-2.10(11)	0.166	
	V	27.98(4)		-1.70(5)					35.500	
	V+LM	27.97(4)		-1.41(4)				-10.21(105)	34.300	
	HC+LM	28.26(2)		-1.41(4)		15.18(92)		-10.12(64)	2.120	
P(1)	SC+LM	28.29(2)		-1.41(4)		18.55(107)	22.16	-10.12(65)	2.140	
	SDV+LM	31.07(1)	7.24(1)	-1.46(4)	-0.06(3)			-9.28(14)	0.484	
	SDHC+LM	31.06(1)	7.30(1)	-1.46(4)	-0.06(3)	1.01(12)		-9.30(13)	0.445	
SF6	HT+LM	30.45(1)	12.25(2)	-1.46(4)	-0.06(3)	21.51(104)		0.78(1)	-9.49(11)	0.381
	V	19.29(3)		-3.80(16)					34.400	
	V+LM	19.29(3)		-3.66(17)				-7.66(123)	34.400	
	HC+LM	19.60(1)		-3.65(8)		8.67(24)		-7.66(29)	0.807	
P(17)	SC+LM	19.65(1)		-3.64(6)		11.45(24)	22.16	-7.64(30)	0.845	
	SDV+LM	20.69(1)	3.66(2)	-3.65(8)	-0.56(3)			-0.83(34)	0.959	
	SDHC+LM	20.18(1)	2.69(1)	-3.89(5)	-0.65(3)	3.37(6)		-2.39(11)	0.299	
	HT+LM	20.17(1)	3.00(1)	-3.88(3)	-0.71(3)	7.69(6)		0.22(1)	-2.47(10)	0.290

## 5. Conclusions and perspectives

We have shown that the Hartmann-Tran profile, recently recommended by IUPAC [45] for high resolution spectroscopy is able to fit measured spectra of CO in various perturbers for large pressure ranges with a precision of better than 0.2 % of the peak absorption. This study confirms the capability of the HT profile to accurately represent observed line shapes for various molecular systems, making the use of this model completely compatible with the precision requirement of current Earth remote sensing experiments.

Because of different approximations used in the model, the fitted line shape parameters do not exactly reflect the underlying physics and should be considered as effective. Nevertheless, they give good indications of the contribution of the various mechanisms that contribute to the line shape. *Ab initio* calculations such as molecular dynamic simulations or quantum calculations may bring detailed information on the underlying physics and should be helpful to improving phenomenological models such as the HT profile. Information obtained from *ab initio* calculations can be used to determine the relative contribution of the various higher-order effects to the line shape and to explain the different behaviors of the P(1) and P(17) lines, for instance. This type of information can also be used to constrain fitted parameters in measured spectra with the HT profile [67]. This approach should help to decrease the numerical correlation between line shape parameters, resulting in parameters that would be more physically-meaningful.

### Acknowledgement:

This work was supported by the NIST Greenhouse Gas Measurement and Climate Sciences Program.

### References

- [1] Wójtewicz S, Stec K, Masłowski P, Cygan A, Lisak D, Trawiński RS, et al. Low pressure line-shape study of self-broadened CO transitions in the (3←0) band. *J Quant Spectrosc Radiat Transf* 2013;130:191–200. doi:10.1016/j.jqsrt.2013.06.005.
- [2] Bouanich JP, Blanquet G. Pressure broadening of CO and OCS spectral lines. *J Quant Spectrosc Radiat Transf* 1988;40:205–20. doi:10.1016/0022-4073(88)90115-X.
- [3] Duggan P, Sinclair PM, Le Flohic MP, Forsman JW, Berman R, May AD, et al.

- Testing the validity of the optical diffusion coefficient: Line-shape measurements of CO perturbed by N<sub>2</sub>. *Phys Rev A* 1993;48:2077–83. doi:10.1103/PhysRevA.48.2077.
- [4] Duggan P, Sinclair PM, May AD, Drummond JR. Line-shape analysis of speed-dependent collisional width inhomogeneities in CO broadened by Xe, N<sub>2</sub>, and He. *Phys Rev A* 1995;51:218–24.
- [5] Henry A, Hurtmans D, Margottin-Maclou M, Valentin A. Confinement narrowing and absorber speed dependent broadening effects on CO lines in the fundamental band perturbed by Xe, Ar, Ne, He and N<sub>2</sub>. *J Quant Spectrosc Radiat Transf* 1996;56:647–71. doi:10.1016/S0022-4073(96)00118-5.
- [6] Sinclair PM, Duggan P, Berman R, May AD, Drummond JR. Line Broadening, Shifting, and Mixing in the Fundamental Band of CO Perturbed by N<sub>2</sub> at 301 K. *J Mol Spectrosc* 1997;181:41–7. doi:10.1080/00268976.2013.839062.
- [7] Berman R, Sinclair PM, May AD, Drummond JR. Spectral profiles for atmospheric absorption by isolated lines: A comparison of model spectra with P- and R-branch lines of CO in N<sub>2</sub> and Ar. *J Mol Spectrosc* 1999;198:283–90. doi:10.1006/jmsp.1999.7887.
- [8] Henry A, Hurtmans D. Collision narrowing and speed dependent effect on broadening in vibration rotation line profiles perturbed by different buffer gases up to one atmosphere - difficulties in these analyses coming from the quality of the tunable diode laser emission. *Spectrochim Acta - Part A* 1999;55:1967–86. doi:10.1016/S1386-1425(99)00069-4.
- [9] Priem D, Rohart F, Colmont J-M, Wlodarczak G, Bouanich J-P. Lineshape study of the  $J = 3 \leftarrow 2$  rotational transition of CO perturbed by N<sub>2</sub> and O<sub>2</sub>. *J Mol Struct* 2000;517–518:435–54. doi:10.1080/00268976.2013.839062.
- [10] Predoi-Cross A, Bouanich JP, Benner DC, May AD, Drummond JR. Broadening, shifting, and line asymmetries in the  $2 \leftarrow 0$  band of CO and CO–N<sub>2</sub>: Experimental results and theoretical calculations 2000;113:158–68. doi:10.1016/j.jms.2005.10.003.
- [11] Predoi-Cross A, Hnatovsky C, Strong K, Drummond JR, Chris Benner D. Temperature dependence of self- and N<sub>2</sub>-broadening and pressure-induced shifts in the  $3 \leftarrow 0$  band of CO. *J Mol Struct* 2004;695–696:269–86. doi:10.1016/j.molstruc.2003.12.043.
- [12] Sung KY, Varanasi P. Intensities, collision-broadened half-widths, and collision-

- induced line shifts in the second overtone band of  $^{12}\text{C}^{16}\text{O}$ . *J Quant Spectrosc Radiat Transf* 2004;83:445–58. doi:Doi 10.1016/S0022-4073(03)00015-3.
- [13] Colmont JM, Nguyen L, Rohart F, Wlodarczak G. Lineshape analysis of the  $J=3 \leftarrow 2$  and  $J=5 \leftarrow 4$  rotational transitions of room temperature CO broadened by  $\text{N}_2$ ,  $\text{O}_2$ ,  $\text{CO}_2$  and noble gases. *J Mol Spectrosc* 2007;246:86–97. doi:DOI 10.1016/j.jms.2007.08.003.
- [14] Malathy Devi V, Chris Benner D, Smith MAH, Mantz AW, Sung K, Brown LR, et al. Spectral line parameters including temperature dependences of self- and air-broadening in the  $2 \leftarrow 0$  band of CO at  $2.3\mu\text{m}$ . *J Quant Spectrosc Radiat Transf* 2012;113:1013–33. doi:10.1016/j.jqsrt.2012.02.010.
- [15] Predoi-Cross A, Esteki K, Rozario H, Naseri H, Latif S, Thibault F, et al. Theoretical and revisited experimentally retrieved He-broadened line parameters of carbon monoxide in the fundamental band. *J Quant Spectrosc Radiat Transf* 2016;184:322–40. doi:10.1016/j.jqsrt.2016.08.007.
- [16] BOUANICH J-P. Determination experimentale des largeurs et des déplacements des raies de la bande  $0 \rightarrow 2$  de CO perturbé par les gaz rares (He, Ne, Ar, Kr, Xe) 1972;12:1609–15.
- [17] Boissoles J, Boulet C, Robert D, Green S. IOS and ECS line coupling calculation for the CO–He system: Influence on the vibration–rotation band shapes. *J Chem Phys* 1987;87:3436. doi:10.1063/1.452988.
- [18] Green S, Boissoles J, Boulet C. Accurate collision-induced line-coupling parameters for the fundamental band of CO in He: Close coupling and coupled states scattering calculations. *J. Quant. Radiat Transf* 1988;39:33–42. doi:10.1016/0022-4073(88)90017-9.
- [19] Duggan P, Sinclair P, Berman R, May A, Drummond JR. Testing Lineshape Models: Measurements for  $v=1-0$  CO Broadened by He and Ar. *J Mol Spectrosc* 1997;186:90–8. doi:10.1006/jmsp.1997.7420.
- [20] Luo C, Wehr R, Drummond JR, May AD, Thibault F, Boissoles J, et al. Shifting and broadening in the fundamental band of CO highly diluted in He and Ar: A comparison with theory. *J Chem Phys* 2001;115:2198–206. doi:10.1063/1.1383049.

- [21] Mantz AW, Henry A, Valentin A. Stabilized Tunable Diode Laser Measurements of the P(2) Line in the  $^{13}\text{CO}$  Fundamental Band Broadened by Helium at Temperatures between 11.5 and 298.6 K. *J Mol Spectrosc* 2001;207:113–9. doi:10.1006/jmsp.2001.8328.
- [22] Henry A, Claveau C, Valentin A, Hurtmans D, Mantz AW. Confinement Narrowing of the R(0) Line in the  $^{13}\text{CO}$  Fundamental Band Broadened by Helium from Room Temperature down to 40 K. *J Mol Spectrosc* 2002;214:28–34. doi:10.1006/jmsp.2002.8576.
- [23] Valentin A, Henry A, Claveau C, Hurtmans D, Mantz AW. Line profile study down to 80 K of R(7) in the  $^{13}\text{CO}$  (1–0) band perturbed by Ar and  $^{13}\text{CO}$  collisional cooling with He at 6.9 K. *Mol Phys* 2004;102:1793–802. doi:10.1080/00268970412331287007.
- [24] Mantz AW, Malathy Devi V, Chris Benner D, Smith MAH, Predoi-Cross A, Dulick M. A multispectrum analysis of widths and shifts in the 2010–2260  $\text{cm}^{-1}$  region of  $^{12}\text{C}^{16}\text{O}$  broadened by Helium at temperatures between 80 and 297 K. *J Mol Struct* 2005;742:99–110. doi:10.1016/j.molstruc.2004.11.094.
- [25] Thibault F, Mantz AW, Claveau C, Henry A, Valentin A, Hurtmans D. Broadening of the R(0) and P(2) lines in the  $^{13}\text{CO}$  fundamental by helium atoms from 300 K down to 12 K: Measurements and comparison with close-coupling calculations. *J Mol Spectrosc* 2007;246:118–25. doi:10.1016/j.jms.2007.09.001.
- [26] Sinclair PM, Duggan P, Berman R, Drummond JR, May AD. Line Broadening in the Fundamental Band of CO in CO-He and CO-Ar Mixtures. *J Mol Spectrosc* 1998;191:258–64.
- [27] Thibault F, Martinez RZ, Domenech JL, Bermejo D, Bouanich JP. Raman and infrared linewidths of CO in Ar. *J Chem Phys* 2002;117:2523. doi:10.1063/1.1494975.
- [28] Wehr R, Vitcu A, Ciuryło R, Thibault F, Drummond J, May AD. Spectral line shape of the P(2) transition in CO-Ar: Uncorrelated ab initio calculation. *Phys Rev A* 2002;66:1–7. doi:10.1103/PhysRevA.66.062502.
- [29] Mantz AW, Thibault F, Cacheiro JL, Fernandez B, Pedersen TB, Koch H, et al. Argon broadening of the  $^{13}\text{CO}$  R(0) and R(7) transitions in the fundamental band at temperatures between 80 and 297 K: Comparison between experiment and theory. *J Mol Spectrosc* 2003;222:131–41. doi:10.1016/S0022-2852(03)00200-5.

- [30] Yamada KMT, Abe H. The line broadening and shift effects on the CO  $J = 5-4$  transition at 576 GHz induced by collisions with rare gases. *J Mol Spectrosc* 2003;217:87–92. doi:10.1016/S0022-2852(02)00045-0.
- [31] Wehr R, Ciuryło R, Vitcu A, Thibault F, Drummond JR, May AD. Dicke-narrowed spectral line shapes of CO in Ar: Experimental results and a revised interpretation. *J Mol Spectrosc* 2006;235:54–68. doi:10.1016/j.jms.2005.10.009.
- [32] Wehr R, Vitcu A, Thibault F, Drummond JR, May AD. Collisional line shifting and broadening in the fundamental P-branch of CO in Ar between 214 and 324 K. *J Mol Spectrosc* 2006;235:69–76. doi:10.1016/j.jms.2005.10.004.
- [33] Bouanich JP, Bermejo D, Domenech JL, Martinez RZ, Santos J. Pressure-Induced Lineshifts in the  $2 \leftarrow 0$  Band of CO Self-Perturbed and Perturbed by He, Kr, O<sub>2</sub>, and N<sub>2</sub>. *J Mol Spectrosc* 1996;179:22–31. doi:10.1006/jmsp.1996.0180.
- [34] Markov VN, Golubiatnikov GY, Savin VA, Sergeev DA, Guarnieri A, Mäder H. Line broadening and shifting studies of the  $J = 5 \leftarrow 4$  transition of carbon monoxide perturbed by CO, N<sub>2</sub>, and O<sub>2</sub>. *J Mol Spectrosc* 2002;212:1–5. doi:10.1006/jmsp.2001.8504.
- [35] Markov V., Sergeev D. Broadening and shifting studies of  $J=5\leftarrow 4$  carbon monoxide line perturbed by Ne, Ar, and Kr. *J Mol Spectrosc* 2004;223:106–7. doi:10.1016/j.jms.2003.10.003.
- [36] Predoi-Cross A, Rohart F, Bouanich JP, Hurtmans D. Xenon-broadened CO line shapes in the fundamental band at 349 K. *Can J Phys* 2009;87:485–98. doi:10.1139/P08-068.
- [37] Dicke RH. The Effect of Collisions upon the Doppler Width of Spectral Lines. *Phys Rev* 1953;89:472–3.
- [38] Galatry L. Simultaneous effect of doppler and foreign gas broadening on spectral lines. *Phys Rev* 1961;122:1218–23. doi:10.1103/PhysRev.122.1218.
- [39] Nelkin M, Ghatak A. Simple binary collision model for Van Hove's  $G_s(r,t)^+$ . *Phys Rev* 1964;135:A4–9.
- [40] Rautian SG, Sobel'man IL. The effect of collisions on the Doppler broadening of spectral lines. *Sov Phys Uspekhi* 1967;9:701–16.

- [41] Berman PR. Collisional Width and Shift. *J Quant Spectrosc Radiat Transf* 1972;12:1331–42.
- [42] Ward J, Cooper J, Smith EW. Correlation Effects in the Theory of Classical Theory 1974;14:555–90.
- [43] Ciuryło R, Szudy J. Speed-dependent pressure broadening and shift in the soft collision approximation. *J Quant Spectrosc Radiat Transf* 1997;57:411–23. doi:10.1016/S0022-4073(96)00078-7.
- [44] Ngo NH, Lisak D, Tran H, Hartmann JM. An isolated line-shape model to go beyond the Voigt profile in spectroscopic databases and radiative transfer codes. *J Quant Spectrosc Radiat Transf* 2013;129:89–100. doi:10.1016/j.jqsrt.2013.05.034.
- [45] Tennyson J, Bernath PF, Campargue A, Császár AG, Daumont L, Gamache RR, et al. Recommended isolated-line profile for representing high-resolution spectroscopic transitions (IUPAC technical report). *Pure Appl Chem* 2014;86:1931–43. doi:10.1515/pac-2014-0208.
- [46] Pine AS. Asymmetries and correlations in speed-dependent Dicke-narrowed line shapes of argon-broadened HF. *J Quant Spectrosc Radiat Transf* 1999;62:397–423. doi:10.1016/S0022-4073(98)00112-5.
- [47] Rohart F, Mader H, Nicolaisen H. Speed dependence of rotational relaxation induced by foreign gas collisions: Studies on CH<sub>3</sub>F by millimeter wave coherent transients. *J Chem Phys* 1994;101:6475–86. doi:10.1063/1.468342.
- [48] Ciuryło R, Pine AS. Speed-dependent line mixing profiles. *J Quant Spectrosc Radiat Transf* 2000;67:375–93. doi:10.1016/S0022-4073(00)00030-3.
- [49] Rosenkranz P. Shape of the 5 mm oxygen band in the atmosphere. *IEEE Trans Antennas Propag* 1975;23:498–506.
- [50] Hodges JT, Layer HP, Miller WW, Scace GE. Frequency-stabilized single-mode cavity ring-down apparatus for high-resolution absorption spectroscopy. *Rev Sci Instrum* 2004;75:849–63. doi:10.1063/1.1666984.
- [51] Lin H, Reed ZD, Sironneau VT, Hodges JT. Cavity ring-down spectrometer for high-fidelity molecular absorption measurements. *J Quant Spectrosc Radiat Transf* 2015;161:11–20. doi:10.1016/j.jqsrt.2015.03.026.

- [52] Courtois J, Bielska K, Hodges JT. Differential cavity ring-down spectroscopy 2013;30:1486–95.
- [53] Lance B, Blanquet G, Walrand J, Bouanich J. On the Speed-Dependent Hard Collision Lineshape Models: Application to  $C_2H_2$  Perturbed by Xe. *J Mol Spectrosc* 1997;185:262–71. doi:10.1006/jmsp.1997.7385.
- [54] Benner DC, Rinsland CP, Devi VM, Smith MAH, Atkins D. A multispectrum nonlinear least squares fitting technique. *J Quant Spectrosc Radiat Transf* 1995;53:705–21. doi:10.1016/0022-4073(95)00015-D.
- [55] Hartmann J-M, Boulet C, Robert D. Collisional effects on molecular spectra. Laboratory experiments and models, consequences for applications. Amsterdam: Elsevier; 2008.
- [56] Hirschfelder J, Curtiss C, Bird R. *Molecular Theory of Gases Liquids*. New York: John Wiley and Sons; 1967.
- [57] Larcher G, Landsheere X, Schwell M, Tran H. Spectral shape parameters of pure  $CO_2$  transitions near  $1.6\mu m$  by tunable diode laser spectroscopy. *J Quant Spectrosc Radiat Transf* 2015;164:82–8. doi:10.1016/j.jqsrt.2015.05.013.
- [58] Le T, Fissiaux L, Lepère M, Tran H. Isolated line shape of methane with various collision partners. *J Quant Spectrosc Radiat Transf* 2016;185:27–36. doi:10.1016/j.jqsrt.2016.07.017.
- [59] Kowzan G, Stec K, Zaborowski M, Wójtewicz S, Cygan A, Lisak D, et al. Line positions, pressure broadening and shift coefficients for the second overtone transitions of carbon monoxide in argon. *J Quant Spectrosc Radiat Transf* 2017;191:46–54. doi:10.1016/j.jqsrt.2016.12.035.
- [60] De Vizia MD, Castrillo A, Fasci E, Moretti L, Rohart F, Gianfrani L. Speed dependence of collision parameters in the  $H_2^{18}O$  near-IR spectrum: Experimental test of the quadratic approximation. *Phys Rev A* 2012;85:1–8. doi:10.1103/PhysRevA.85.062512.
- [61] Lisak D, Cygan A, Bermejo D, Domenech JL, Hodges JT, Tran H. Application of the Hartmann-Tran profile to analysis of  $H_2O$  spectra. *J Quant Spectrosc Radiat Transf* 2015;164:221–30. doi:10.1016/j.jqsrt.2015.06.012.

- [62] Hartmann JM, Tran H, Ngo NH, Landsheere X, Chelin P, Lu Y, et al. Abinitio calculations of the spectral shapes of CO<sub>2</sub> isolated lines including non-Voigt effects and comparisons with experiments. *Phys Rev A* 2013;87:13403. doi:10.1103/PhysRevA.87.013403.
- [63] Tran H, Domenech JL. Spectral shapes of Ar-broadened HCl lines in the fundamental band by classical molecular dynamics simulations and comparison with experiments. *J Chem Phys* 2014;141:64313. doi:10.1063/1.4892590.
- [64] Hartmann JM, Boulet C, Auwera J Vander, El Hamzaoui H, Capoen B, Bouazaoui M. Line broadening of confined CO gas: From molecule-wall to molecule-molecule collisions with pressure. *J Chem Phys* 2014;140. doi:10.1063/1.4864205.
- [65] Seleznev AF, Fedoseev GV, Koshelev MA, Tretyakov MY. Shape of collision-broadened lines of carbon monoxide. *J Quant Spectrosc Radiat Transf* 2015;161:171–9. doi:10.1016/j.jqsrt.2015.04.011.
- [66] Rohart F, Nguyen L, Buldyreva J, Colmont JM, Wlodarczak G. Lineshapes of the 172 and 602 GHz rotational transitions of HC15N. *J Mol Spectrosc* 2007;246:213–27. doi:10.1016/j.jms.2007.09.009.
- [67] Wcisło P, Gordon IE, Tran H, Tan Y, Hu SM, Campargue A, et al. The implementation of non-Voigt line profiles in the HITRAN database: H<sub>2</sub> case study. *J Quant Spectrosc Radiat Transf* 2016;177:75–91. doi:10.1016/j.jqsrt.2016.01.024.

**Figure Captions**

Fig.1: Top panel: Measured absorption spectra of the 3-0 P(1) (left) and P(17) (right) lines of  $^{12}\text{C}^{16}\text{O}$  broadened by He, obtained from FS-CRDS measurements at room temperature and various total pressures. The spectra are normalized for unity peak absorption with the fitted base losses are removed. Because of the precise agreement between measurements and model, the fitted data points are not shown. Bottom panels: residuals (observed – calculated) obtained from multispectrum fits of the measured spectra with the considered line shape models (see text).

Fig.2: Top panel: absorption spectra of the 3-0 P(1) (left) and P(17) (right) lines of  $^{12}\text{C}^{16}\text{O}$  broadened by Ar, measured at room temperature and various total pressures. The spectra are normalized for unity peak absorption with the fitted base losses are removed. Bottom panels: residuals obtained from multispectrum fits of the measured spectra with the different considered line shape models.

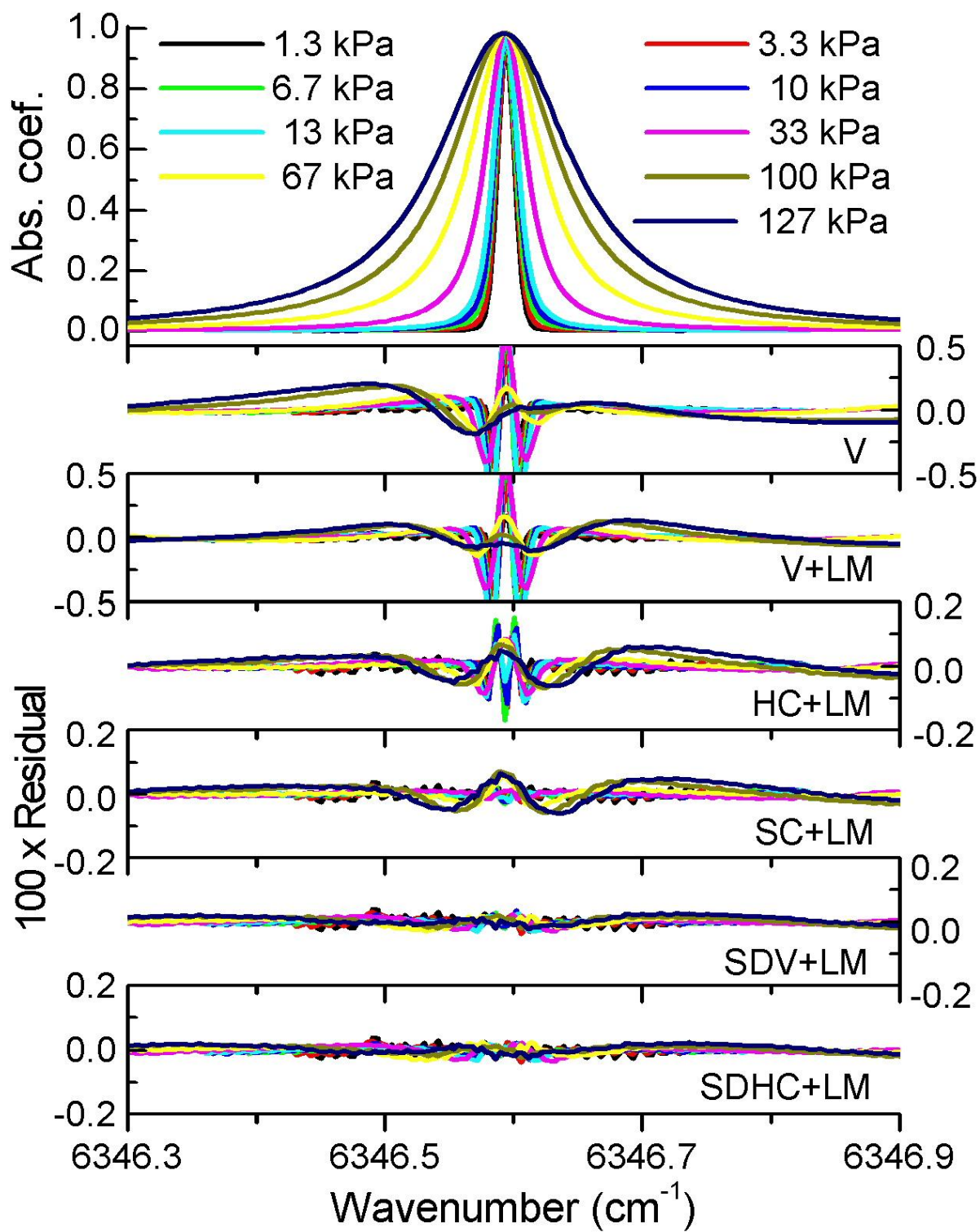
Fig.3: Same as figure 2 above but for CO in Kr

Fig.4: Same as figure 3 but for CO in  $\text{SF}_6$

**Highlights**

- The Harmann-Tran profile was compared to measured spectra of CO in various perturbers
- High resolution and high S/N of two lines of CO were measured with a FS-CRDS system
- Spectra measured over a large pressure range were simultaneously analyzed
- The HTP is capable to represent the measurements within 0.1% of the peak absorption

Fig.1



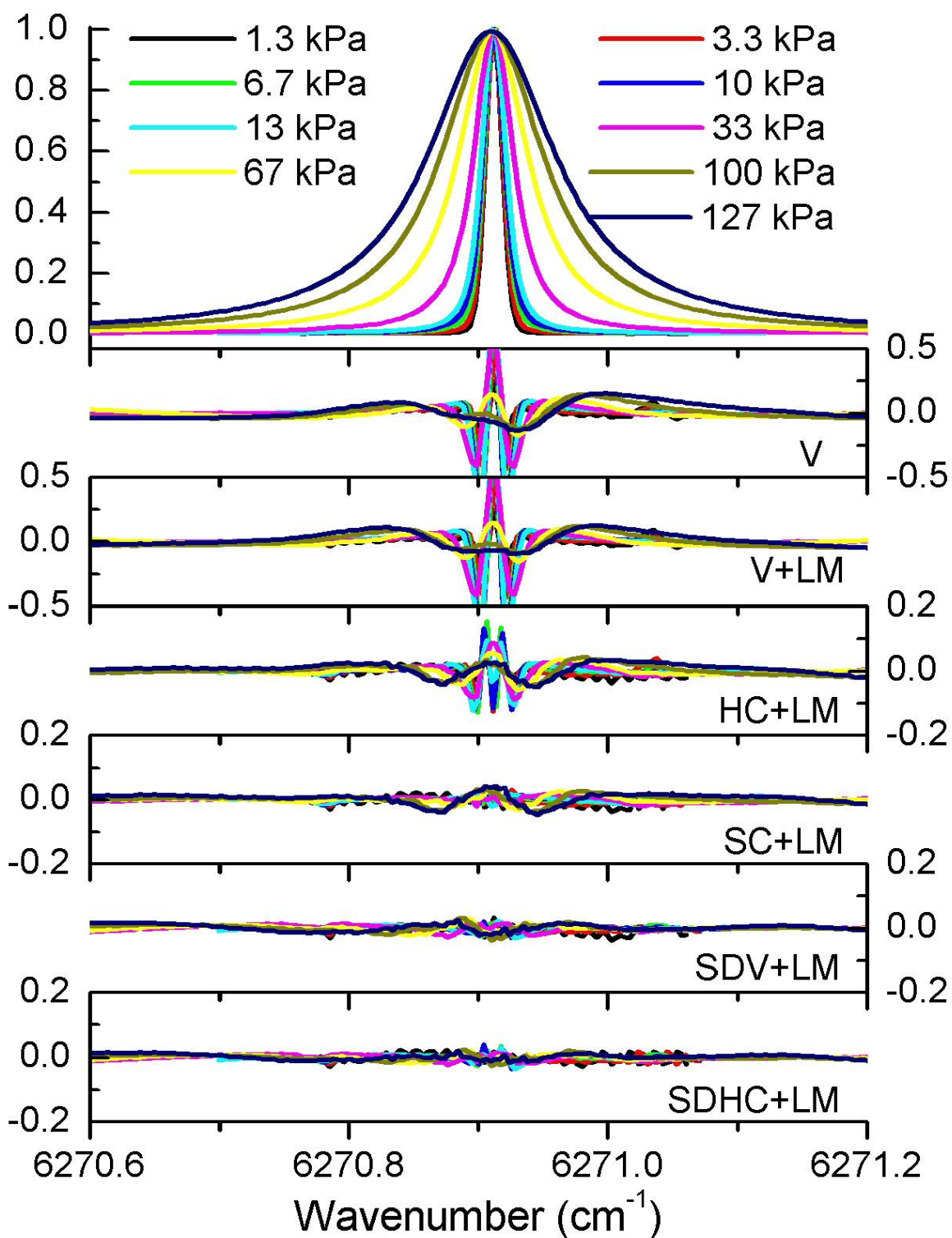
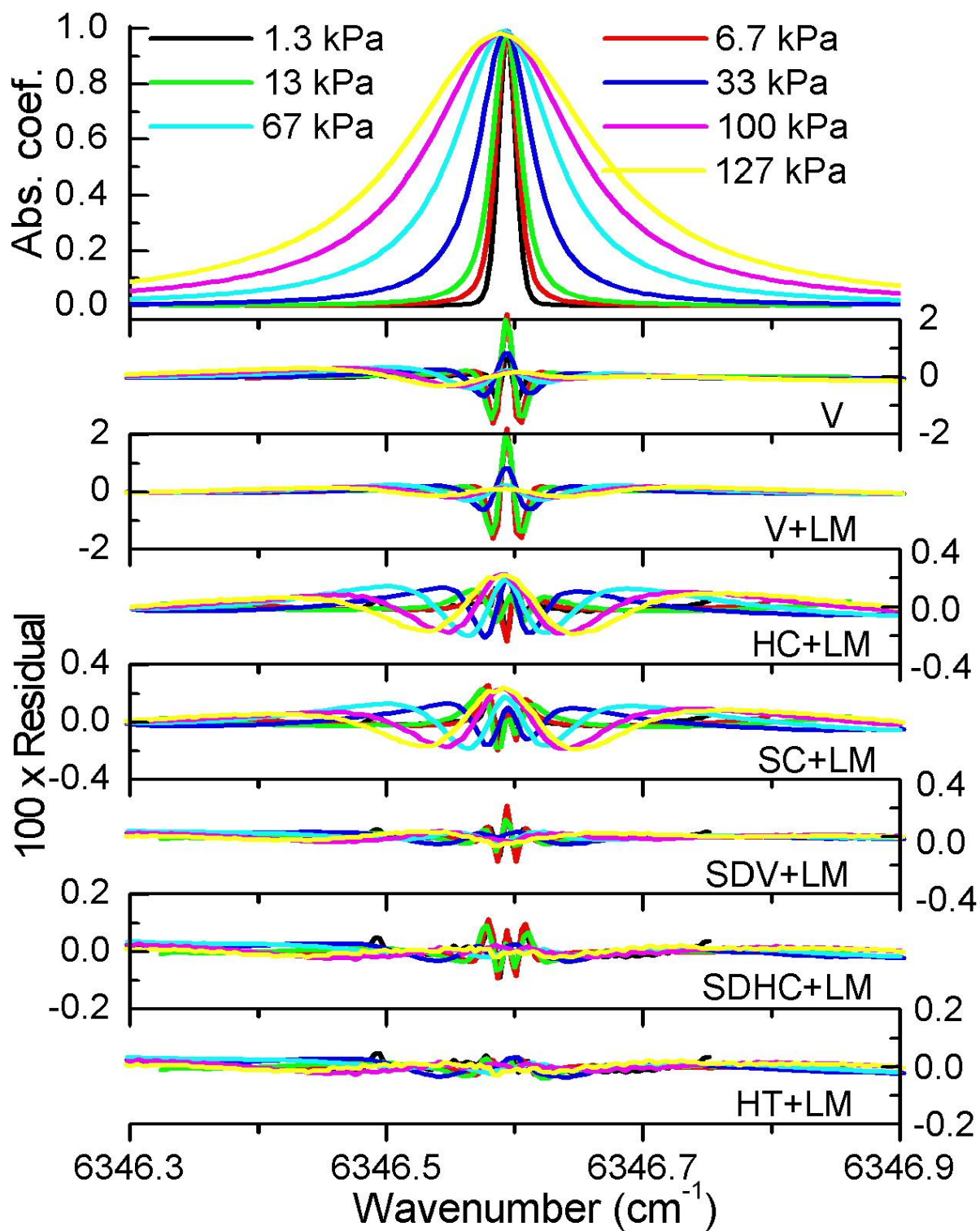


Fig 2



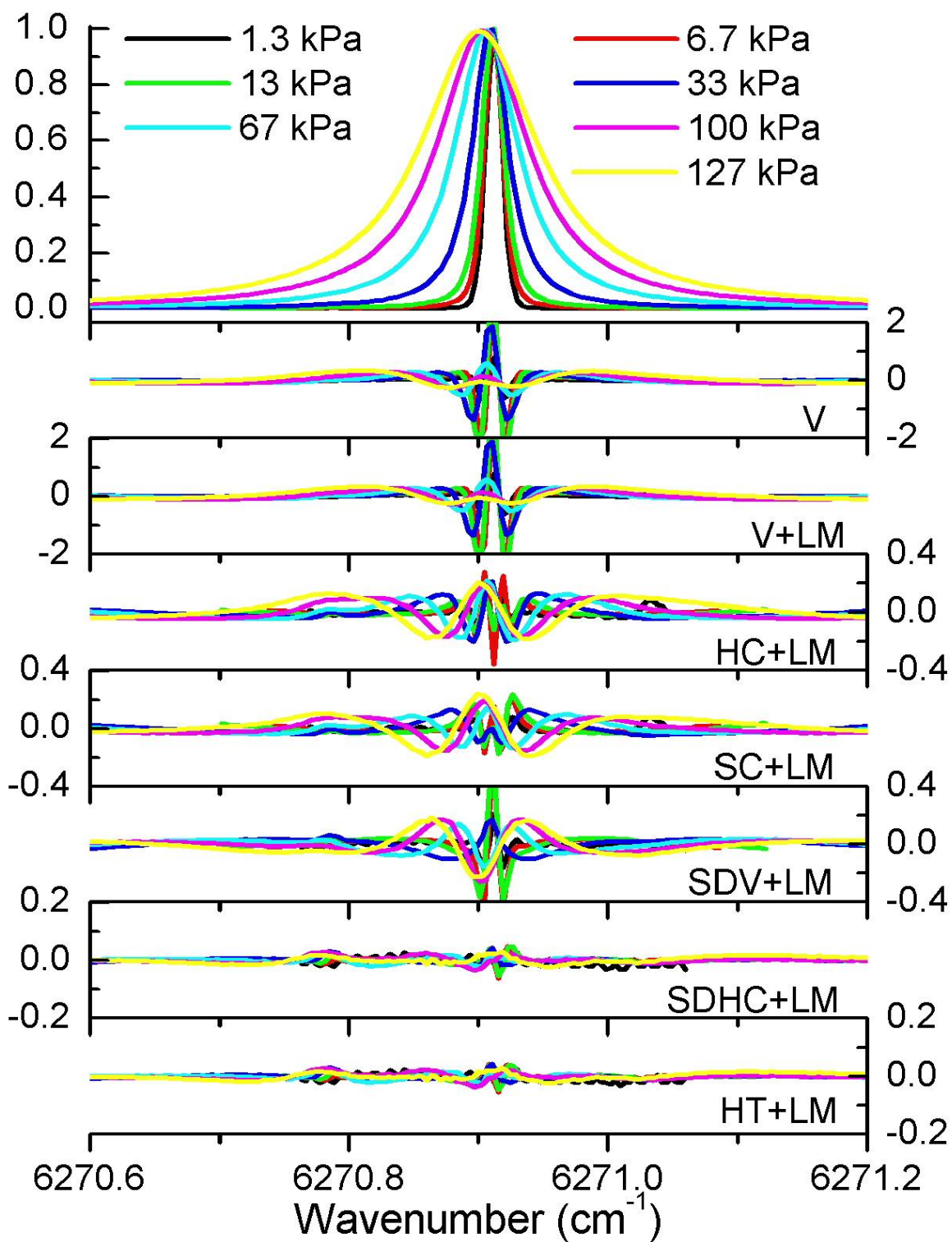
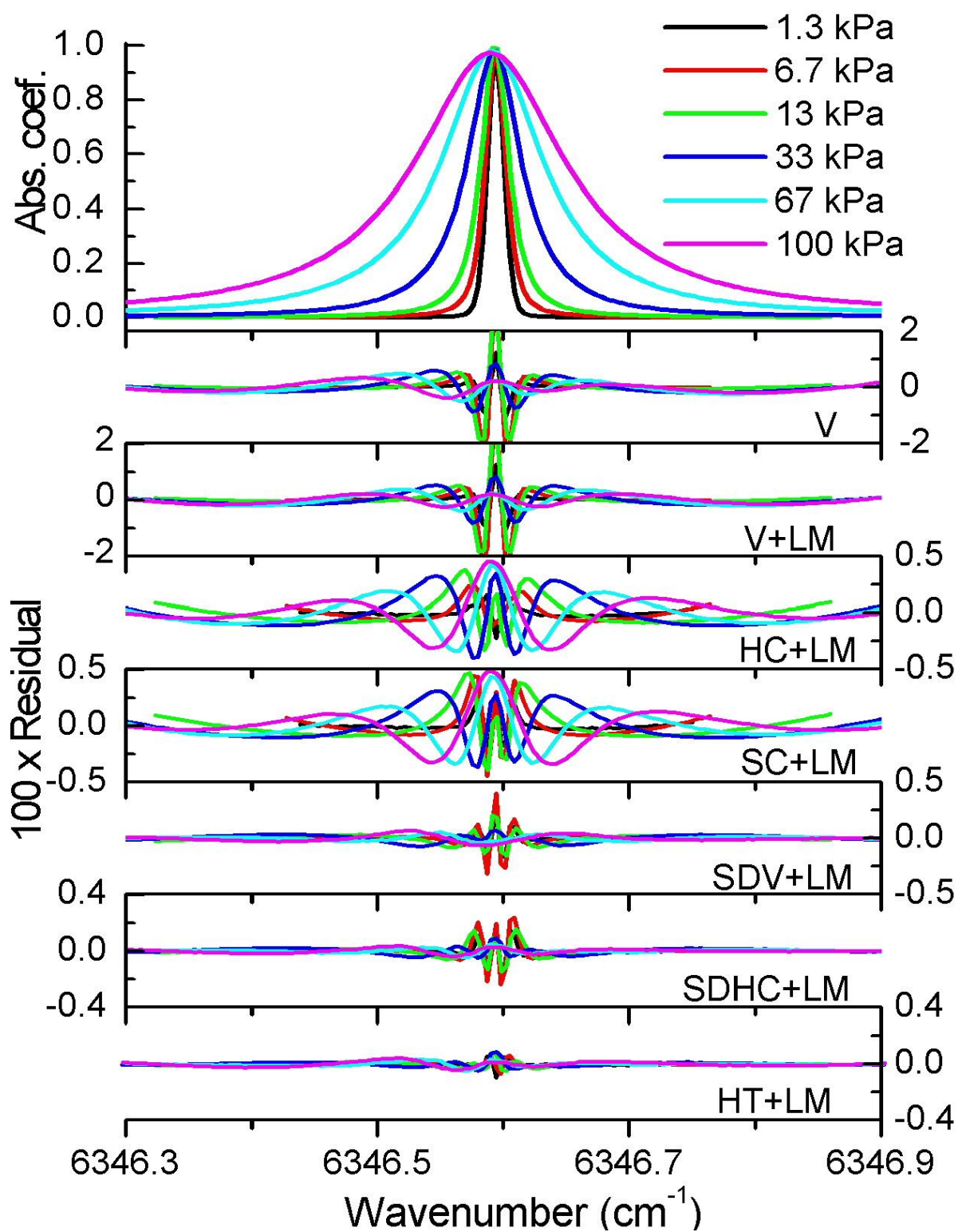


Fig 3



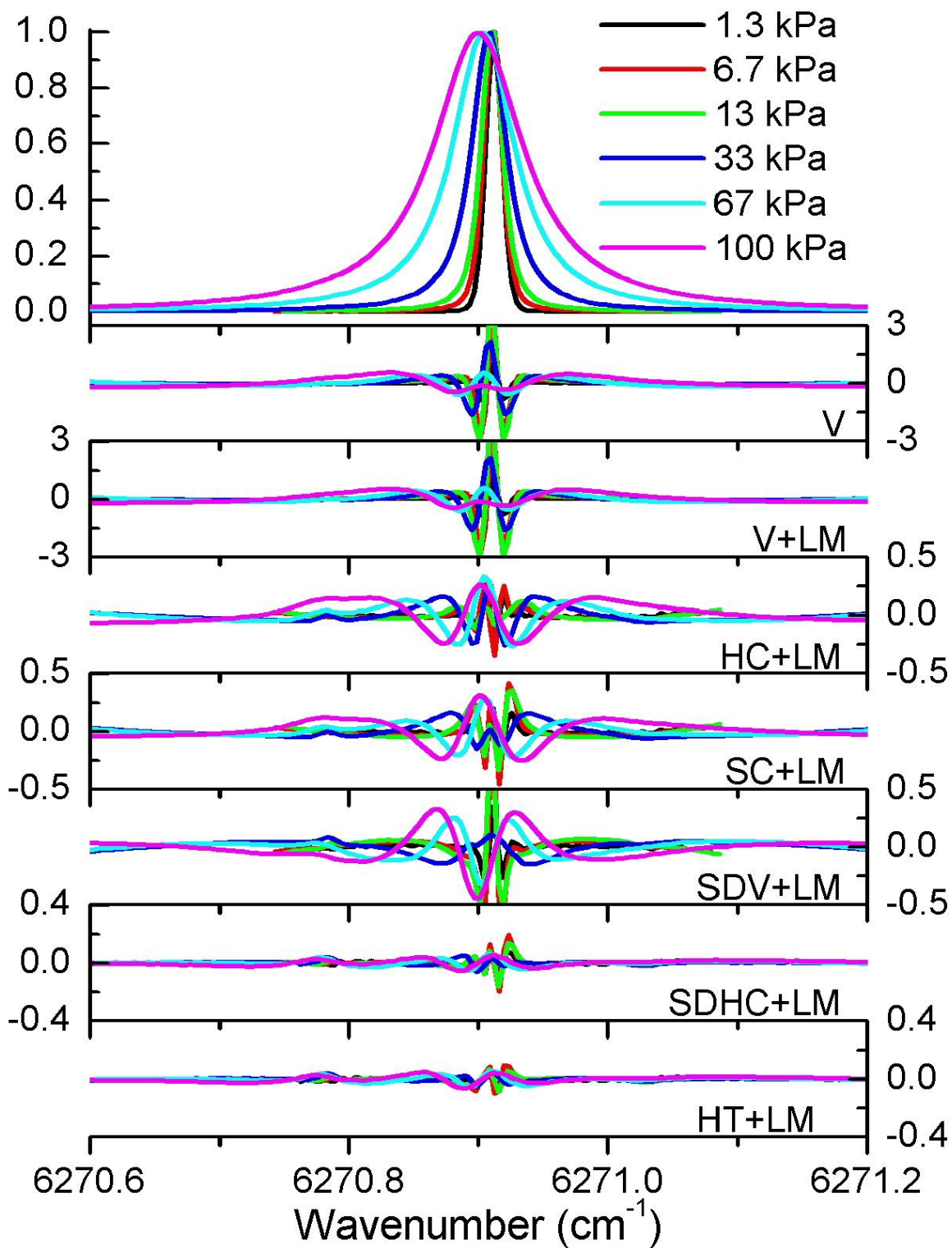


Fig 4

